Available online at www.sciencedirect.com
ScienceDirect
Icarus ••• (••••) •••–•••
ICARUS
www.elsevier.com/locate/icarus

Direct measurement of the size, shape, and pole of 511 Davida with Keck AO in a single night

A.R. Conrad [a,*], C. Dumas [b], W.J. Merline [c], J.D. Drummond [d], R.D. Campbell [a], R.W. Goodrich [a], D. Le Mignant [a], F.H. Chaffee [a], T. Fusco [e], S.H. Kwok [a], R.I. Knight [f]

[a] *W.M. Keck Observatory, 65-1120 Mamalahoa Highway, Kamuela, HI 96743, USA*
[b] *ESO Very Large Telescope (VLT), European Southern Observatory, Alonso de Cordova 3107, Vitacura Casilla 19001, Santiago 19, Chile*
[c] *Southwest Research Institute, 1050 Walnut Street, Suite 300, Boulder, CO 80302, USA*
[d] *Starfire Optical Range, Directed Energy Directorate, Air Force Research Laboratory, Kirtland AFB, NM 87117-5776, USA*
[e] *Office National d'Etudes et de Recherches Aerospatiales (ONERA), DOTA-E, BP 72, F-92322 Chatillon, France*
[f] *University of Hawaii, 200 W. Kawili St., Hilo, HI 96720-4091, USA*

Received 28 December 2006; revised 7 May 2007

Abstract

Using the high-quality data set of 165 images taken at 11 epochs over the 5.13 h rotation of the large C-type Asteroid 511 Davida, we find the dimensions of its triaxial ellipsoid model to be $357 \pm 2 \times 294 \pm 2 \times 231 \pm 50$ km. The images were acquired with the adaptive optics system on the 10 m Keck II telescope on December 27, 2002. The a and b diameters are much better determined than previously estimated from speckle interferometry and indirect measurements, and our mean diameter, $(abc)^{1/3} = 289 \pm 21$ km, is 19% below previous estimates. We find the pole to lie within 2° of [RA = 295°; Dec = 0°] or in Ecliptic coordinates [$\lambda = 297°$; $\beta = +21°$], a significant improvement to the pole direction. Otherwise, previous determinations of the axial ratios agree with our new results. These observations illustrate that our technique of finding the dimensions and pole of an asteroid from its changing projected size and shape is very powerful because it can be done in essentially one night as opposed to decades of lightcurves. Average departures of 3% (5 km) of the asteroid's mean radius from a smooth outline are detected, with at least two local positive-relief features and at least one flat facet showing approximately 15 km deviations from the reference best-fit ellipsoid. The facet is reminiscent of large global-scale craters on Asteroid 253 Mathilde (also a C-type) when seen edge-on in close-up images from the NEAR mission flyby. We show that giant craters (up to 150 km diameter, the size of the largest facets seen on Davida) can be expected from the impactor size distribution, without likelihood of catastrophic disruption of Davida.

Keywords: Asteroids, rotation; Adaptive optics

1. Introduction

The physical and statistical study of asteroids requires reliable knowledge of their precise size, shape, and pole orientation. By studying the size and shape of these bodies, we hope to learn more about their gross structure and better understand asteroid collisions, the major geological process shaping these objects. An accurate size measurement leads to an improved albedo measurement, a parameter that is key to understanding composition. A precise shape measurement, in particular, can help us understand the history of large, but subcatastrophic, impacts on a body and how the body's response to such impacts may relate to its internal structure and composition. It has been hypothesized, by Housen et al. (1999), for example, that very porous asteroids, such as 253 Mathilde, have a very different response to giant impacts than denser targets (e.g., S-types), with the crater being formed largely by compaction rather than ejection of material. By studying a variety of asteroid shapes in detail, we can constrain the possible variabilities seen within asteroid taxonomic types, and determine systematics, if any, among them.

* Corresponding author.
E-mail address: aconrad@keck.hawaii.edu (A.R. Conrad).

0019-1035/$ – see front matter
doi:10.1016/j.icarus.2007.05.004

Furthermore, having accurate sizes is crucial for the determination of asteroid volume, and hence density, in the cases where the mass can be determined, e.g., from the presence of a satellite (Merline et al., 2002). Uncertainty in asteroid size is the overwhelming uncertainty in asteroid densities in such cases. This has further implications in understanding the internal structure from porosity determinations (Britt et al., 2002, 2006).

Methods to measure the size of an asteroid can be divided into indirect and direct techniques, the former being comprised of radiometric methods and lightcurve studies, and the latter of spacecraft observations, radar, stellar occultations, speckle interferometry, and adaptive optics (AO). A good introduction to these various techniques (except AO and spacecraft observations) is the chapter in *Asteroids II* by Magnusson et al. (1989). Davida is presented there as an observation or calibration standard because it has been extensively observed, it has smooth symmetrical lightcurves, and because different techniques converge on the determination of its shape and pole direction. In the present paper, we show that the overall shape of the asteroid is well represented by a triaxial ellipsoid and support the use of Davida as a standard with respect to shape and size determination. We also provide means to predict the rotational phase of the asteroid for future observational epochs.

The most popular indirect method for determining the shape and rotational pole location of an asteroid is through studying its lightcurves (e.g., Kaasalainen et al., 2003), but this requires multiple measurements spanning many years. On the other hand, a direct technique that can lead not only to the shape and pole of an asteroid, but to its dimensions as well, over only one or two nights, was developed for speckle interferometry by Drummond et al. (1985), and can also be applied to AO observations (Drummond et al., 1998; Drummond, 2006). We use this method to determine the triaxial dimensions and pole of Asteroid 511 Davida from AO observations at eleven rotational phases using the 10 m Keck II telescope. The high spatial resolution achieved using the 10 m telescope, combined with multiple samples, afford views of substantial departures (both high and low) from a smooth reference ellipsoid, of roughly 15 km (10% of asteroid mean radius), revealing at least two positive-relief features and at least one large relative 'deficit,' which we call here a facet.

Magnusson (1989) began compiling a list of asteroid axial ratios and spin vectors that is now maintained by A. Kryszczynskaat on a web site.[1] The entries for Davida from this database are compared with our direct measurements throughout the paper.

2. Observations

On December 27, 2002, we collected rotationally and spatially resolved, nearly diffraction-limited, K'-band (2.1 μm) images of Davida at 11 light-time corrected epochs (Table 1), using the second generation near infrared camera (NIRC2) on the Keck II telescope. [See Wizinowich et al. (2000) for the initial report on AO at Keck.] Davida, a large C-type asteroid, was near opposition at that time. The 11 epochs were spaced approximately evenly in time across a full rotation, and at each epoch we took 15 images over a 5 min span. Observations of a nearby star of similar airmass and magnitude were interlaced with the Davida observations to calibrate the point spread function (PSF). The background was removed by subtracting a sky frame and the individual images were then flat-field corrected and combined with a sub-pixel shift-and-add (Fig. 1).

Table 1
Observational log

Epoch	UT[a]	UT − UT$_1$	$\psi_{\rm rel}$	$\Delta\psi_{\rm rel}$	$\psi_{\rm true}$[b]
1	8:08:39	0:00:00	0°	0°	−68.46°
2	8:28:52	0:20:12	23.63	23.63	−44.83
3	8:55:47	0:47:08	55.12	31.49	−13.25
4	9:33:54	1:25:15	99.71	44.59	31.25
5	9:53:31	1:44:52	122.66	22.95	54.20
6	10:21:59	2:13:20	155.95	33.29	87.49
7	10:52:35	2:43:56	191.73	35.78	123.27
8	11:13:07	3:04:28	215.75	24.02	147.29
9	11:36:37	3:27:57	243.22	27.47	174.76
10	12:15:11	4:06:32	288.34	45.12	219.88
11	12:50:34	4:41:55	329.73	41.39	261.27

[a] Light-time corrected.
[b] Rotational phase $\psi_{\rm true} = 0°$ at 9.12 UT corresponds to the maximum cross-sectional area.

Epochs 6 and 10 were observed at H (1.6 μm) and K'; the remaining nine epochs were observed at K' only. When observing at K' in good seeing conditions, the first generation adaptive optics system on Keck II delivers approximately 50 milliarcsecond (diffraction limited) resolution elements. We used the NIRC2 narrow plate scale, oriented North-up (±0.01°), which, at 10.0 ± 0.1 milliarcseconds per pixel, resulted in resolution elements spanning 5 detector pixels. This corresponds to a resolution of approximately 58 km on the Davida surface, with approximately 6 resolution elements across the diameter (28 pixels in this mode) and 25 resolution elements covering the entire disk (616 pixels). The 40 milliarcsecond angular resolution at H corresponds to a resolution of approximately 46 km, with approximately 7 resolution elements across the diameter and 38 resolution elements covering the disk. Davida was at a distance of 1.617 AU from Earth, within 6 days of opposition, and at a solar phase angle of 2.9° (illuminated fraction 99.9%). The next time Davida will come this close will be in the year 2030.

3. Triaxial ellipsoid analysis

Assuming that Davida is a triaxial ellipsoid with radii $a > b > c$ rotating about its short axis, then as it rotates it will project a series of ellipses of apparent semi-major axes α and semi-minor axes β, where the long axis will make an angle γ with an axis (the line of nodes) perpendicular to the direction of its rotational pole. These apparent ellipse parameters will depend on the latitude of the sub-Earth point, θ, and the rotational phase, $\psi_{\rm true}$, where the true rotational phase is related to the relative rotational phase with a constant, $\psi_{\rm true} = \psi_{\rm rel} - \psi_0$, and where $\psi_0 = 68.5°$ is found from the non-linear fits below. The true rotational phase in Table 1 is the rotational phase since the maximum cross-sectional area at 9.12 UT. Drummond et

[1] http://www.astro.amu.edu.pl/Science/Asteroids/.

Please cite this article in press as: A.R. Conrad et al., Direct measurement of the size, shape, and pole of 511 Davida with Keck AO in a single night, Icarus (2007), doi:10.1016/j.icarus.2007.05.004

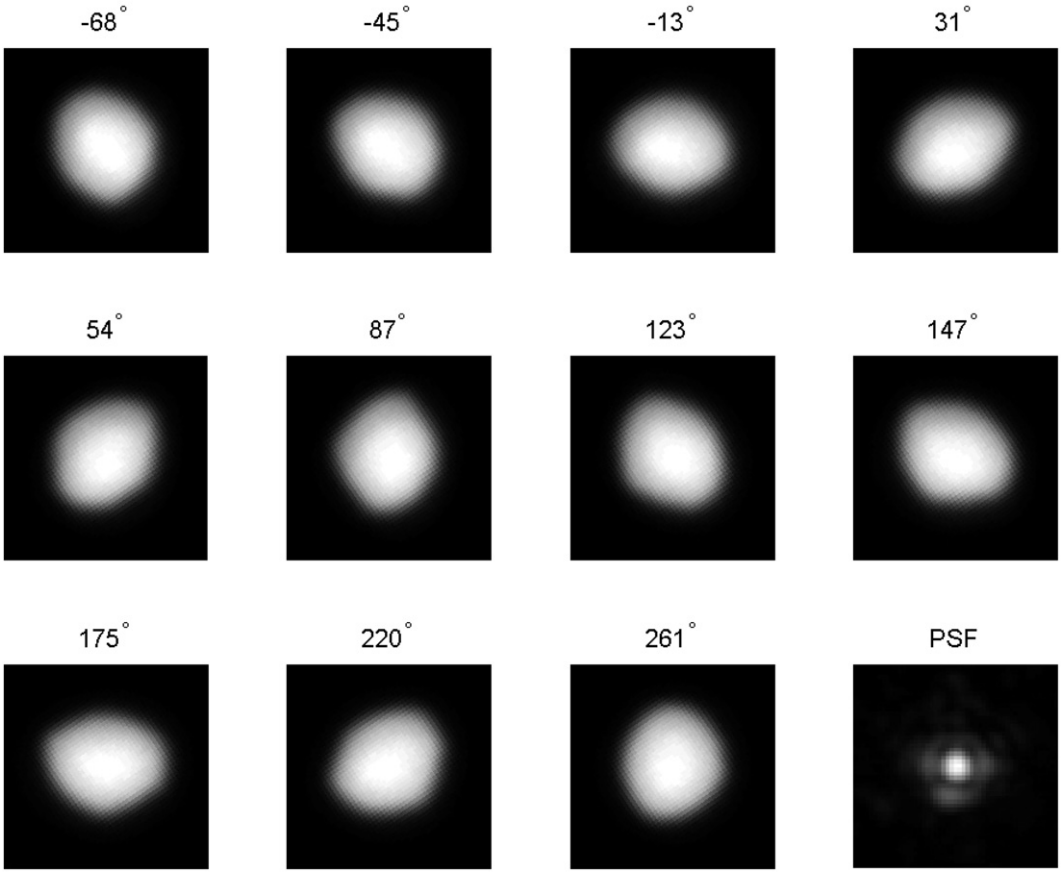

Fig. 1. Adaptive optics images of 511 Davida at eleven rotational phases obtained with the 10 m Keck II telescope. The images are rotated so that the projection of the asteroid's North Pole is up (inclined by 23° to the plane of the image), the celestial North Pole is 34° counterclockwise from up, and East is 90° further counterclockwise. The asteroid rotates counterclockwise in this view. Each of the 11 images is the average of 15 K'-band (2.1 μm) images that are combined by shift-and-add at each epoch. At the top of each figure is the true rotational phase. At lower right is a sample image of the Keck K' PSF. The asteroid images are displayed with a squared stretch, which shows the hard edges, while the PSF is displayed with a square-root stretch to show the low-light-level structure. Each panel is a $0.5'' \times 0.5''$ square.

al. (1985) and Drummond (2000) list the equations relating the apparent ellipse parameters to triaxial ellipsoid parameters.

The 15 images that were taken at each epoch were sky-subtracted, flat-fielded, removed of bad pixels, and then spatially co-registered using 2-D cross-correlation, and added together to yield a combined, single, averaged image for each epoch. Each of these averaged images were then fit to determine the apparent ellipse parameters for each epoch.

We find the apparent ellipse parameters for each image with three methods, fitting convolved images, fitting deconvolved images, and fitting edges. For reduction purposes, the point spread function for adaptive optics is taken to be Lorentzian in shape (Drummond, 1998, 2000; Drummond et al., 1998). The convolution of the Lorentzian and the asteroid can be fit with a non-linear least squares routine in the Fourier plane, where it becomes the product of a modified Bessel function of the second kind of order 0 (K_0) for the Lorentzian, and a Bessel function of the first kind of order 1 ($2J_1(x)/x$) for the asteroid. The non-linear least squares fit yields the asteroid's apparent semi-major axes and the position angle of the long axis, and the same quantities for the Lorentzian PSF.

For the first method, each of eleven mean images were fit in the Fourier plane for the asteroid and Lorentzian parameters. In general, the PSF from a ground-based telescope without AO can be Gaussian or Lorentzian-like (see Merline and Howell, 1995). With good AO, performance closer to the diffraction limit produces an Airy pattern, which is the PSF of a clear circular aperture. At low Strehls,[2] the PSF has a strong (but variable) Lorentzian component and a weak Airy component. As the Strehl increases, the Airy emerges and the Lorentzian declines. Therefore, as a test of this first method of fitting for the asteroid and a single component Lorentzian PSF, another round of fitting was made, this time using a variable Lorentzian plus a fixed Airy appropriate for the telescope and wavelength as the PSF. These fits gave the same results for the asteroid as the fit with a single component Lorentzian PSF. Therefore, the results from the fit of the asteroid and Lorentz-only PSF were adopted.

A second fit for the ellipse parameters at each rotational phase was made of images deconvolved with the MISTRAL[3] package (Fusco et al., 2002). In this case, fits were made for

[2] The ratio of the peak of the PSF to the peak of a perfect, diffraction limited profile, both normalized to their volume.

[3] MISTRAL: Copyright Conan, Mugnier, Fusco—ONERA 1998–2000.

Please cite this article in press as: A.R. Conrad et al., Direct measurement of the size, shape, and pole of 511 Davida with Keck AO in a single night, Icarus (2007), doi:10.1016/j.icarus.2007.05.004

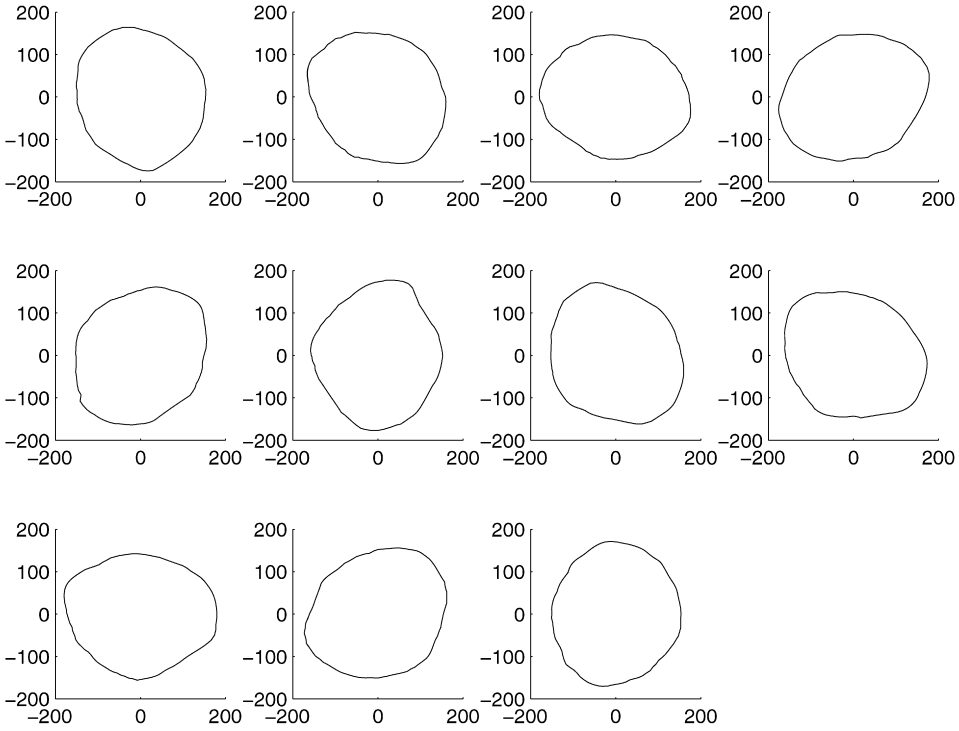

Fig. 2. Outline of Davida as found from Sobel edge-fitting the deconvolved images. Ninety points around the edge are connected by line segments. The orientation is the same as in Fig 1.

just the asteroid in the Fourier domain, and no PSF. The only differences in the results were that a and b came out 1% larger and the angular elements were different by one degree.

For a third fit, we applied a discrete differentiation operator (Sobel, 1973), an edge finder, to the deconvolved images in the image domain in order to mark the edges at every 4° around the circumference. Each of these points was then smoothed with a running average within a 12° interval, i.e., each point was averaged with its two immediate neighbors, and the resulting edge points, still at 4° intervals, were connected with straight lines to produce the limb profiles shown in Fig. 2. With this smoothing, the level of apparent detail in the outlines corresponds to the near diffraction-limited angular resolution available from our observation. Finally, we obtained apparent ellipse parameters at each epoch by fitting an ellipse to the 90 points marking the edge of the asteroid at each rotational phase.

Separately for each of the three sets of fits (two in the Fourier domain and one in the image domain), we used a non-linear least squares program to find the full triaxial ellipsoid from the set of apparent ellipse parameters α, β, and γ for each rotational phase (Drummond et al., 1985; Drummond, 2000). Table 2 gives the solutions for each fit, and a final fit of the mean of the three measurements at each rotational phase as shown in Fig. 3. The UT in Table 2 is light-time corrected and the poles are for J2000. The largest uncertainty is for c because the sub-latitude of the observer, θ, is so high.

There is a normal two-fold ambiguity in locating the pole with our technique. Our accepted pole is listed in Table 2. For the record, the rejected pole lies at [RA = 267°; Dec = −37°] or Ecliptic coordinates [$\lambda = 268°$; $\beta = -14°$] (see next section).

Table 2
Triaxial ellipsoid fits for Davida

	Conv.	Deconv.	Edges	Mean
a (km)	356 ± 2	359 ± 2	355 ± 2	357 ± 2
b (km)	290 ± 2	296 ± 2	297 ± 2	294 ± 2
c (km)	241 ± 36	242 ± 43	191 ± 114	231 ± 50
θ (°)	66 ± 5	66 ± 5	70 ± 6	67 ± 5
PA_{Node} (°)	235 ± 2	236 ± 2	237 ± 2	236 ± 2
ψ_0 UT	9.10 ± 0.03	9.12 ± 0.03	9.13 ± 0.03	9.12 ± 0.03
Eq. pole [RA°; Dec°]	[297; +1]	[296; +1]	[294; −3]	[295; +0]
Pole error radius (°)	2	2	2	2
Ecl. pole [λ°; β°]	[299; +22]	[298; +22]	[295; +19]	[297; +21]

4. Comparison to previous results

Fig. 4 shows our current results for the axial ratios ($a/b = 1.21 \pm 0.01$, $b/c = 1.27 \pm 0.28$) plotted as error bars, along with values previously determined from lightcurves. The means and standard deviations of the previous measures in Fig. 4 are $a/b = 1.24 \pm 0.03$, $b/c = 1.18 \pm 0.11$. While the a/b ratio is well determined, the b/c ratio is less so. Fig. 5 plots the uncertainty around the pole found here, which lies at the southern end of previous determinations. Our uncertainty in the pole position of 2° is smaller than that of previous methods, typically having uncertainties of 5°–10°. Our two ambiguous poles are shown in Fig. 5. We rejected the pole that lies far from the consensus region of previous determinations.

Conrad et al. (2006) performed a preliminary analysis of this data set and concluded that the size of Davida had been overestimated by Drummond and Hege (1989). We have quantified that assertion. The Drummond and Hege mean diameter

Please cite this article in press as: A.R. Conrad et al., Direct measurement of the size, shape, and pole of 511 Davida with Keck AO in a single night, Icarus (2007), doi:10.1016/j.icarus.2007.05.004

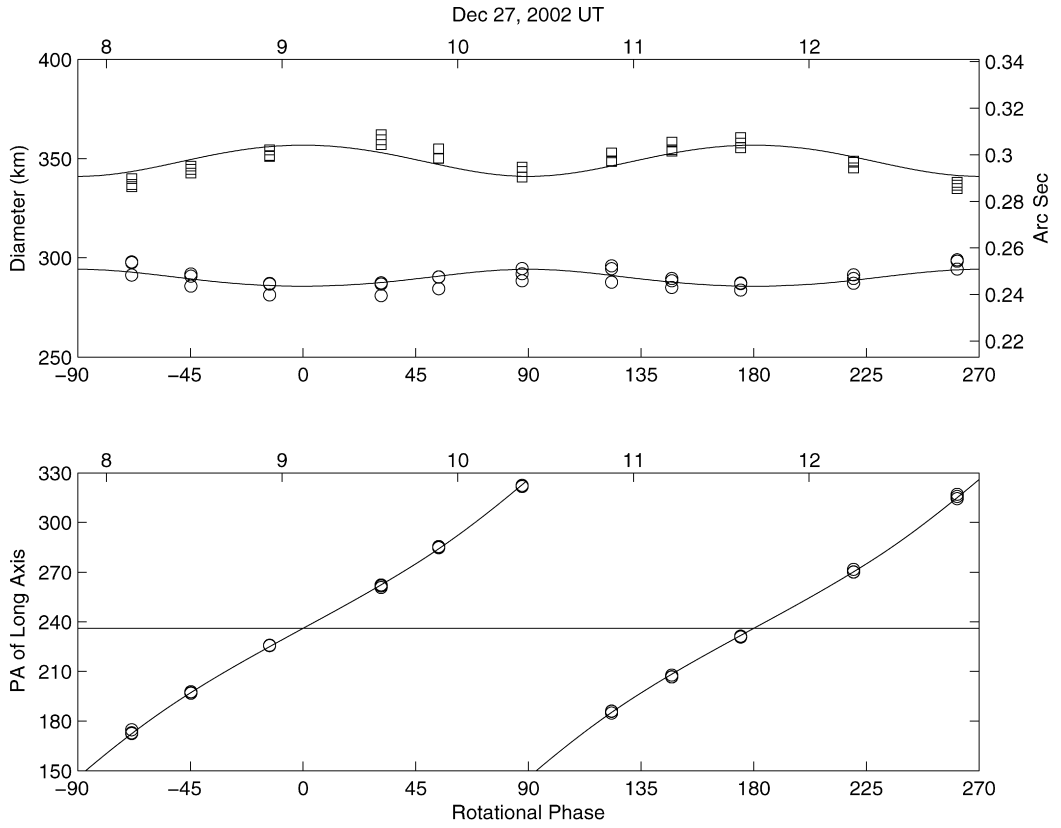

Fig. 3. Triaxial ellipsoid fit to measured ellipse parameters. In the upper subplot, each image's long (α, squares) and short (β, circles) axis dimensions from each of the three methods are plotted, with the uncertainties of the observations approximately the size of the symbols. The lines are the prediction for the projected ellipses from the mean triaxial ellipsoid parameters in Table 2. Because the solar phase angle is only 2.9°, the lines for the predicted terminator ellipses are indistinguishable. The lower subplot shows the same for the position angle of the long axis. This figure is corrected for light time travel, i.e., the plot is in the body-centered time frame.

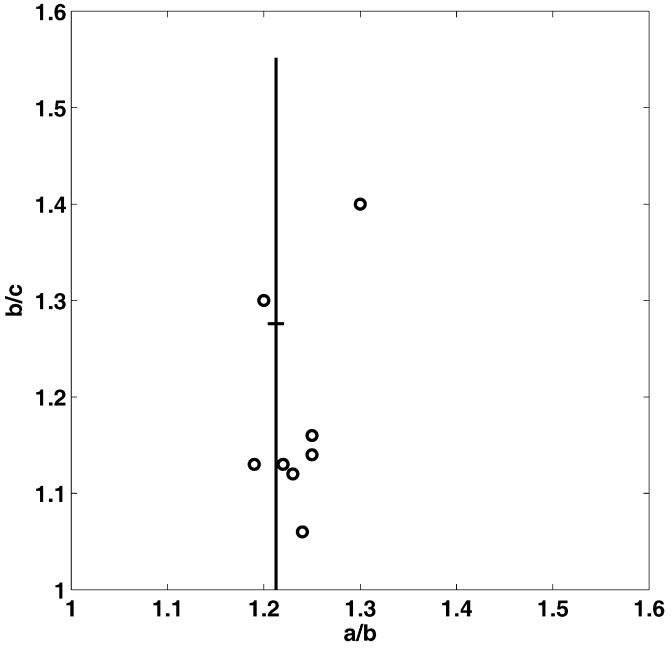

Fig. 4. Axial ratios for Davida. The present results are indicated by the error bars, while circles show the ratios found from lightcurves.

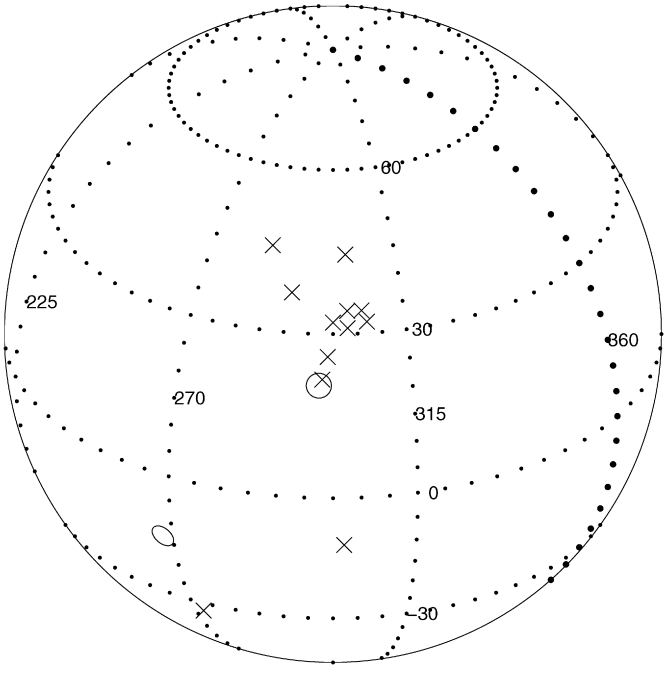

Fig. 5. Pole locations for Davida on the Ecliptic globe. Both circles denote the 2° radius of uncertainty around our two possible poles, and the ×'s mark the positions (without uncertainties) found by previous work, having typical uncertainties of 5°–10°. We resolve our pole ambiguity by its proximity to the majority of previous estimates.

Please cite this article in press as: A.R. Conrad et al., Direct measurement of the size, shape, and pole of 511 Davida with Keck AO in a single night, Icarus (2007), doi:10.1016/j.icarus.2007.05.004

of $(abc)^{1/3} = 344 \pm 21$ km ($417 \pm 48 \times 333 \pm 25 \times 292 \pm 34$ km) was 19% larger than our new value, $(abc)^{1/3} = 289 \pm 21$ km. Our new measurement yields a volume that is 60% of the previous value.

The albedo and mean dimension from the Infrared Astronomical Satellite (IRAS; Tedesco, E.F., Veeder, G.J., Fowler, J.W., Chillemi, J.R., 1992. The IRAS Minor Planet Survey—Final Report (PL-TR-92-2049), Phillips Laboratory, Hanscom Air Force Base, MA) for Davida are 0.054 ± 0.002 and 326 ± 5 km, respectively. The latitude of the sub-Earth point on Davida during 1983, the year IRAS was aloft, was around $-62°$. From our ellipsoid model and pole, the mean apparent diameters ($2\sqrt{\alpha\beta}$) for this sub-latitude at maximum and minimum cross-sectional area were 317 and 313 km, respectively. Overall, the mean diameter of 315 km is only 3% smaller than the IRAS measurement, implying that either the asteroid is slightly smaller at these orientations than IRAS found, that the albedo should be increased from 0.054 to 0.058, or some combination of the two. (Increasing our model dimensions by our uncertainties only increases the mean diameter to 321 ± 3 km.) Altogether, we consider the agreement between the IRAS model and ours as excellent.

Furthermore, since Davida's sidereal period is well known, $P = 0.2137235$ days (see footnote 1), with an uncertainty of 1 in the last digit, we can predict the asterocentric geometry for any future Julian date epoch, JD, including the longitude of the sub-Earth point, L, on the asteroid to within 0.29 degrees per year from a given epoch. We define longitudes as measured counterclockwise from one of the long tips of the asteroid while looking down from above its North Pole. The relationship between the longitude of the sub-Earth point as we define it here and the rotational phase ψ in Fig. 3 is $L = 270° - \psi$. While the rotational phase increases with time as the asteroid rotates, the longitudes decrease. Note that times are body-centered; they should always be lighttime corrected for the distance to the asteroid by subtracting 8.31 min/AU from an observation.

Let the pole location in celestial coordinates be given by α_p and δ_p, and the position of the asteroid by α_a and δ_a. The angular distance of the sub-Earth point on the asteroid from the asteroid's South Pole is ζ, and the longitude of the sub-Earth point in an inertial coordinate system is k, given by

$$\zeta = \cos^{-1}\left[\sin\delta_p \sin\delta_a + \cos\delta_p \cos\delta_a \cos(\alpha_p - \alpha_a)\right], \quad (1)$$

$$k = \sin^{-1}\left[(\sin\delta_p \cos\zeta - \sin\delta_a)/(\sin\zeta \cos\delta_p)\right];$$
$$\text{if } \sin(\alpha_p - \alpha_a) < 0,\ k = 180° - k. \quad (2)$$

The sub-Earth latitude is then

$$\theta = \zeta - 90° \quad (3)$$

and the sub-Earth longitude is

$$L = 31.87 - 360(\mathrm{JD} - \mathrm{JD}_0)/P + k, \quad (4)$$

where $\mathrm{JD}_0 = 2452635.88$, corresponding to the time of maximum cross section area in Fig. 3 at 9.12 UT December 27, 2002, when $L = 270°$. Thus Davida's prime meridian is defined to be along the long axis that points to the Earth a quarter of a rotation earlier, at 7.83 UT.

As an example, let us work out the observing geometry for Davida for the Spitzer satellite observations of Lim et al. (2005). They observed Davida on September 22, 2002, between 12:41:15 and 13:13:59 UT. At that time Davida was at RA = 86.65° and Dec = +14.43°. From Eq. (1) $\zeta = 148.5°$, from Eq. (2) $k = 208.5°$, and from Eq. (3) the sub-Earth latitude was $\theta = +58.5$. Subtracting 21.25 min for light-time travel, the Julian dates for the beginning and end times were 2452540.0139 and 2452540.0366, leading to L's of 79.1° to 40.8° with Eq. (4). Using the equations for triaxial ellipsoids given by Drummond et al. (1985), the range of apparent semi-major and semi-minor axes for this θ and these L's are 178–171 and 139–143 km, respectively, giving mean radii ($\sqrt{\alpha\beta}$) of 157–156 km. From their analysis of their radiometric data, Lim et al. derive a mean radius for Davida of 168.6 ± 13.0 km, only slightly greater than (but within their uncertainty of) our prediction.

Our definition of Davida's longitude system is in a right-handed sense and follows the recommendations of the 2003 IAU/IAG Working Group on Cartographic Coordinates and Rotational Elements (Seidelmann et al., 2005). As a final example, let us calculate the sub-Earth longitude on Davida on January 1.5, 2000, if the asteroid is placed at RA $= \alpha_p - 90°$ and $\delta = 0°$ as required in the definition of W by the Working Group. Now W is merely the negative of our L, and since we find $L = 271.26°$ for this situation and epoch, $W = -271.26° = 88.74°$.

Thus, using this set of AO images, we have obtained definitive results for Davida's shape, size and pole that support the notion of this asteroid being a good calibration object. Only its short c dimension might be improved by future observations at a lower sub-Earth latitude.

5. Limb irregularities

In employing the edge-finding technique of Section 3, it became apparent that Davida's limb is irregular on scales of tens of kilometers (see Fig. 2). Orienting the images so that the asteroid's North Pole is up, Fig. 6 shows the reference ellipsoid (the mean from Table 2) at each rotational phase, together with the limb profiles from Fig. 2.

Let us define a position angle ξ that starts at the asteroid's western limb (to the right) and goes around the outline in a counterclockwise direction (WNES). Fig. 6 shows the reference ellipsoid globe at each rotational phase, and a line segment connecting the measured edge points at every 4° of ξ, smoothed with a running average over 12°. Two circles or spots are drawn on the reference ellipsoid beneath two of the most obvious features. Not until the spots reach the limb are these promontories seen in relief. A closer view of frames 6–9 is provided in Fig. 7, where the features are most clearly followed. A facet, or flat area, precedes feature B in rotation. Fig. 8 shows this feature, labeled c, along with the A and B promontories.

Plotting the difference between the edge positions and the reference apparent ellipse as a function of ξ yields the limb profile in Fig. 9. Fig. 10 is a close-up of frames 6–9, but plotting both the reference apparent ellipse radius and the limb obtained

Please cite this article in press as: A.R. Conrad et al., Direct measurement of the size, shape, and pole of 511 Davida with Keck AO in a single night, Icarus (2007), doi:10.1016/j.icarus.2007.05.004

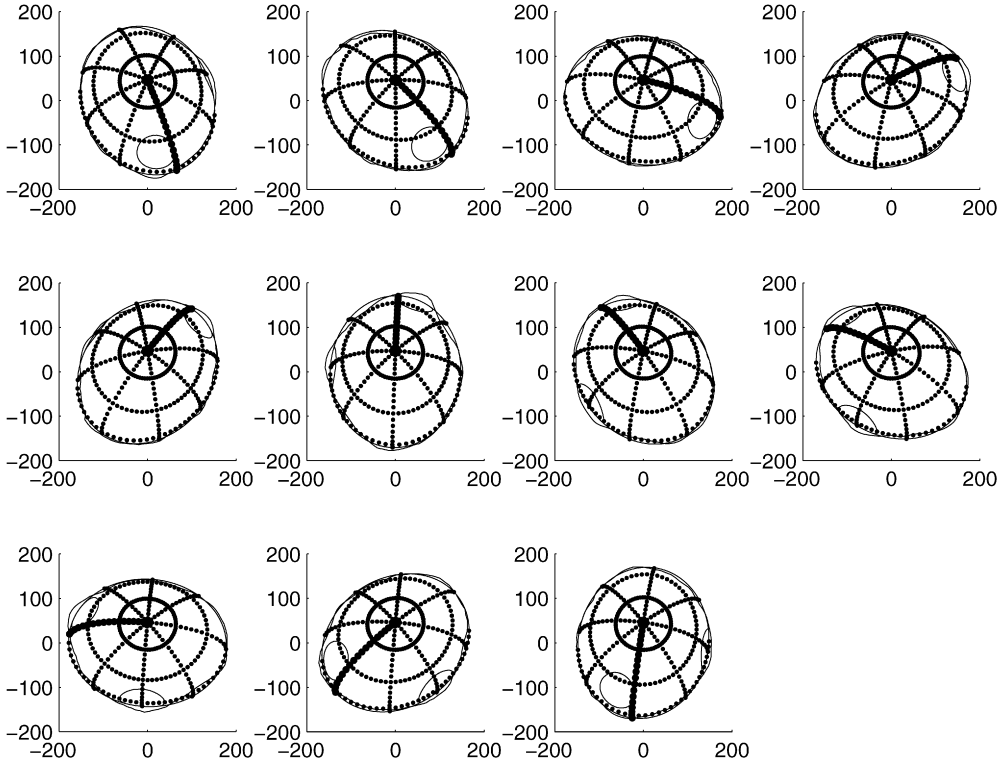

Fig. 6. Rotation of Davida using the mean parameters from Table 2, where the latitude of the sub-Earth point is +67°. The asteroid's irregular outline in Fig. 2 is also drawn for each of these observed rotational phases. A circle is drawn beneath two of the most obvious shape features. We refer to these promontories that rise, set, and rotate appropriately with the body's rotation, as A (at the bottom in the first frame) and B (first seen coming into view in the 6th and 7th frames). When the circles beneath the features lie on the limb, the promontories are best seen in profile, as in frame 6. Celestial north is 34° counterclockwise from the top, and east proceeds counterclockwise from there. The scale is in km. Lines of longitude are indicated every 45° and lines of latitude every 30°. The prime meridian where $L = 0$ is indicated by heavier dots.

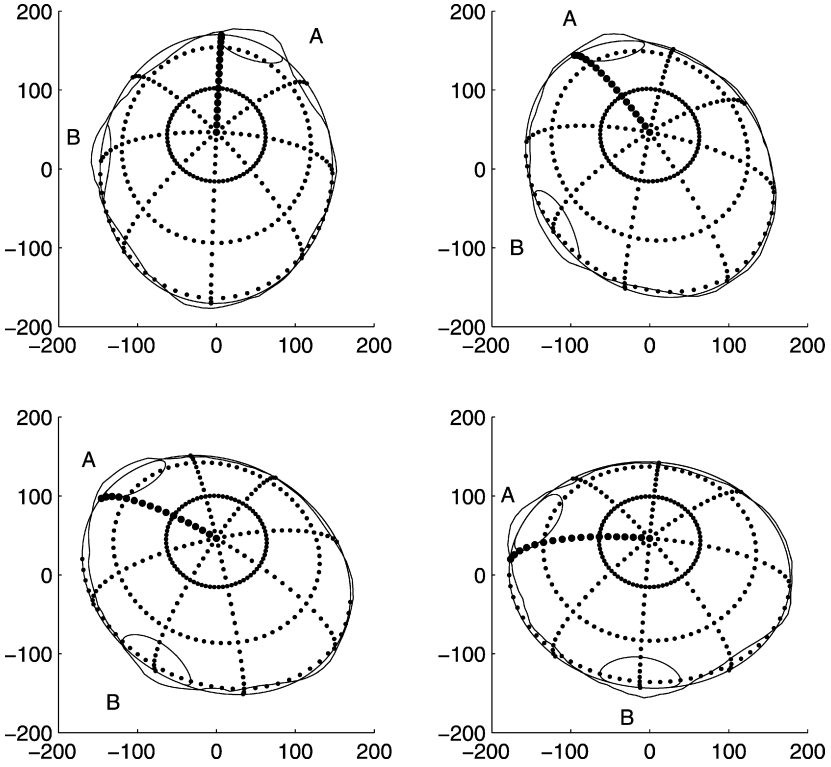

Fig. 7. Close-up of frames 6–9 of Fig. 6 with two features labeled. The parameters of the features are listed in Table 3.

Please cite this article in press as: A.R. Conrad et al., Direct measurement of the size, shape, and pole of 511 Davida with Keck AO in a single night, Icarus (2007), doi:10.1016/j.icarus.2007.05.004

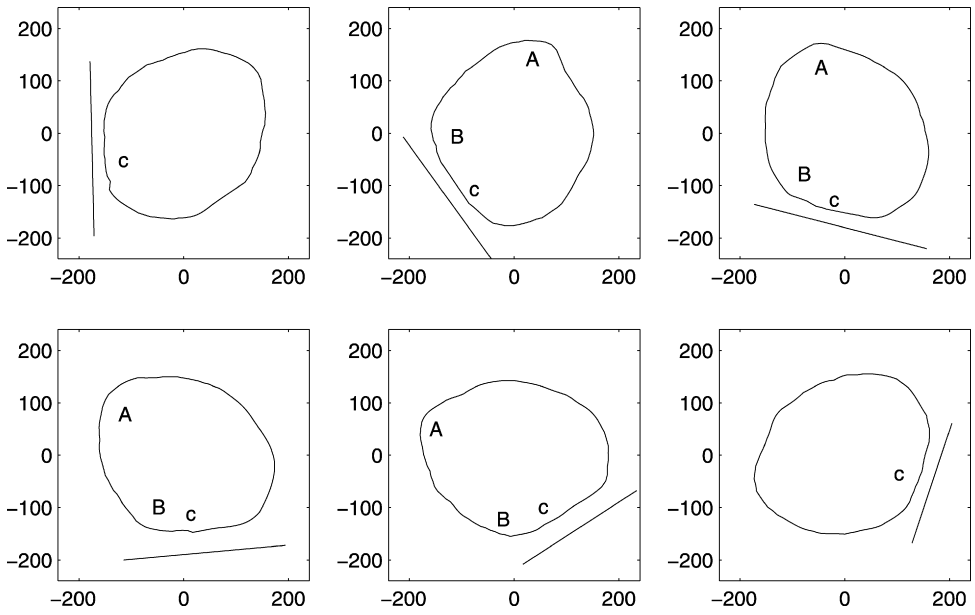

Fig. 8. Frames 5–10 of Fig. 2, showing the facet c. The facet discussed in the text is the flat area in Davida's outline next to the lines in each frame, and spans approximately 150 km. Features A and B from Fig. 7 are also indicated on the inside of the outline of the corresponding frames here.

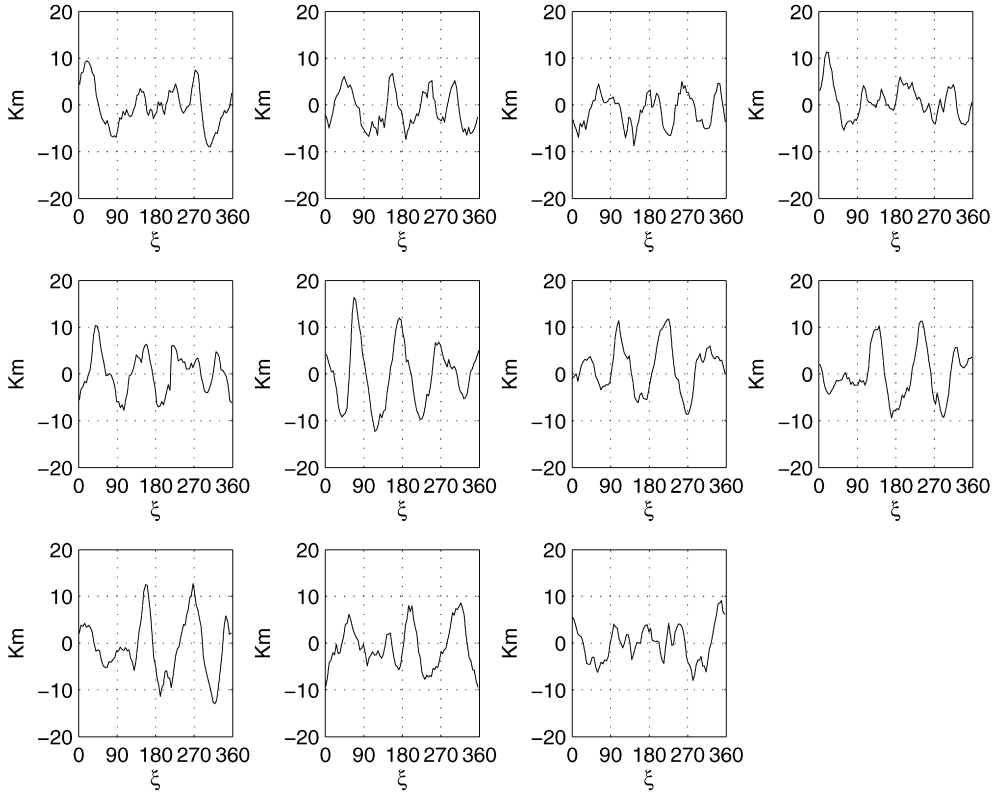

Fig. 9. Relief of limb, corresponding to the views of Fig. 6. The difference between the limb and the reference ellipse is shown in km around the limb of the asteroid. The edges were measured every 4° of ξ (the horizontal scale) starting from the western edge of the asteroid (to the right in Figs. 6 and 7) and proceeding counterclockwise.

from the measured edges. Table 3 contains the estimated longitude, latitude, and size (diameter) of the underlying spots for features A and B, the reference ellipsoid radius at this feature, and the heights of the promontories above this radius. The table also lists similar quantities for facet c, but here the diameter of the feature refers to the extent in longitude of the flat area (see the last frame in Fig. 7 and the corresponding 5th frame in Fig. 8), but this does not necessarily imply that it extends similarly in latitude.

While the standard deviation of all the differences between the edges and the reference ellipse is 5 km, this is only 3% of the mean radius of the outlines, hence it is still valid to assume

Please cite this article in press as: A.R. Conrad et al., Direct measurement of the size, shape, and pole of 511 Davida with Keck AO in a single night, Icarus (2007), doi:10.1016/j.icarus.2007.05.004

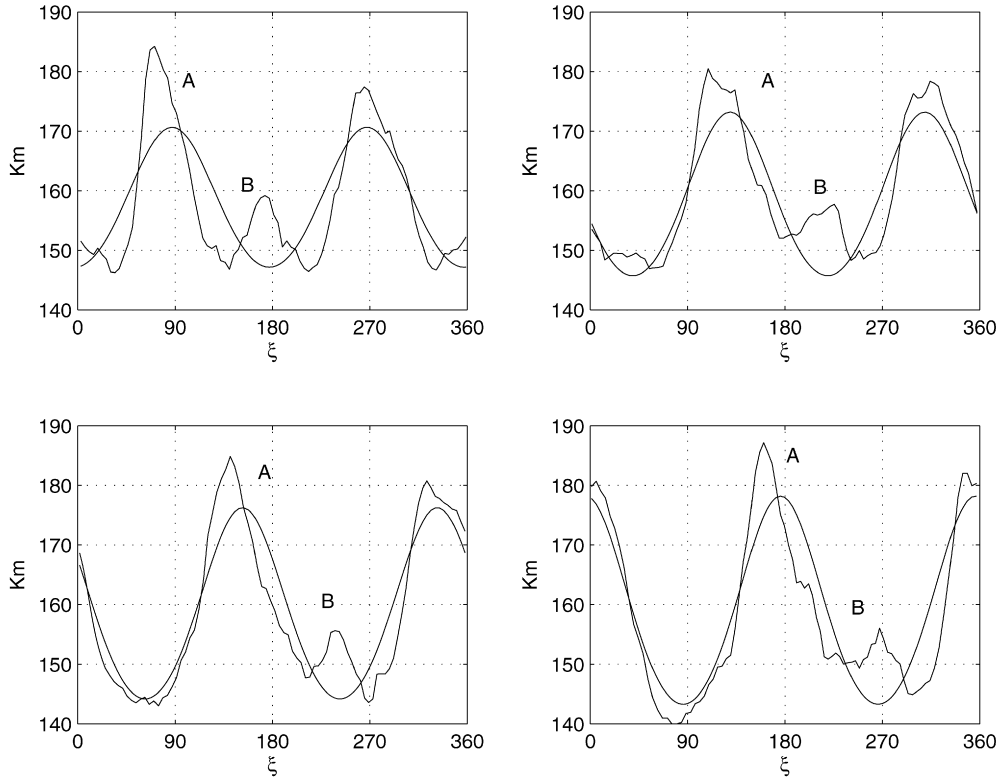

Fig. 10. Limb profile for mean ellipse and edges for frames 6–9 of Fig. 9. Promontories A and B are indicated as rising above the mean ellipse, and facet c is the deficit between the outline and the mean ellipsoid at ξ's greater than B. Yet another feature can also be seen rising above the mean ellipse at ξ's greater than B by about 90°, but is not as easily followed in Figs. 6 and 7.

Table 3
Limb features

Feature	Longitude	Latitude	Diameter (°)	Ellipsoid radius (km)	Height (km)
A	345	+20	30	163	+18
B	90	0	40	147	+12
c	135	0	90	161	−12

that Davida satisfies our assumption of a smooth triaxial ellipsoid. The features extend approximately 15 km above or below the mean radius, corresponding to a departure from smoothness of 10%.

While our linear spatial resolution at the asteroid is about 58 km, fifteen images were acquired at each epoch. Thus, we estimate our random errors to be about 15 km, which corresponds to about 5° along the limb. Smoothing with a running average to 12° eliminates higher frequency noise in the outline, but still allows the detection of the three features we identify here. We do not account for any systematic errors, but the sustained definition of the features during rotation at consistent locations in asterocentric coordinates argues that the features are real.

No surface albedo features that could be confirmed through rotation on the object were detected in either the convolved or deconvolved images. We did not interpret this as being an unusual characteristic of Davida. For example, Mathilde, the only C-type asteroid that has been studied close-up, during the NEAR mission flyby (Veverka et al., 1999), is essentially devoid of any albedo markings or variations. As a result, we used the deconvolved images to extract only the contour of Davida as described above.

6. Comparison with Mathilde

A view of Mathilde (Veverka et al., 1999) is shown in Fig. 11. One can immediately see similarities with our images of Davida. For example, the profile of Mathilde shows very large, flat 'facets,' which turn out to be the tops of large craters, seen edge-on. These extremely large craters on Mathilde were an unexpected discovery of the NEAR mission. Mathilde is essentially saturated with large craters of diameters roughly equal to the asteroid's radius (Chapman et al., 1999). The proximity of these craters forms apparent 'promontories' on Mathilde, relative to what one would consider a reference ellipsoid, and may be analogues of the promontories we see on Davida. Indeed, the most prominent flat facet on Davida, c, is immediately adjacent to promontory feature B, as seen in Fig. 8. Furthermore, another flat facet appears between promontory features A and B. Yet another facet may be seen in the second frame of Fig. 8, adjacent (but trailing in rotation) to A. This facet can be followed over a few frames of Fig. 8, but is most pronounced as a slight concavity to the upper right of the second frame of Fig. 8. When seen precisely edge-on, the large Mathilde craters also exhibit a slightly concave morphology. We expect this apparent shape is the result of having giant craters, of order the target radius, formed on spherical or ellipsoidal targets.

Please cite this article in press as: A.R. Conrad et al., Direct measurement of the size, shape, and pole of 511 Davida with Keck AO in a single night, Icarus (2007), doi:10.1016/j.icarus.2007.05.004

Fig. 11. NEAR image of Asteroid 253 Mathilde. Many of the features on the limb of Davida that we discuss seem analogous to features seen on the limb of Mathilde. The outline on the right is provided for comparison with the Davida profiles given in Fig. 8.

Thus, many of the qualitative features seen on Mathilde are enticingly similar to features of our Davida profiles, and the Davida facets may also be manifestations of giant craters. However, Davida is a much larger asteroid, and it is reasonable to ask whether the yet larger craters implied could even be possible on Davida. First, we note the relative sizes of the apparent facets on each object. The largest crater on Mathilde has a diameter about 33 km, roughly 1.25 times the average radius (26.5 km) of the asteroid. The largest facet on Davida appears to be about 150 km, about 1.04 times our derived average radius. So the scales of these facets are comparable, relative to the size of the target. There are about five craters larger than 20 km diameter that are visible on the approximate 60% of Mathilde that was imaged (Chapman et al., 1999). Davis (1999) points out that the 33 km crater on Mathilde would have required an impactor of diameter 1.3 km. Asphaug (2000) estimates that this impactor would have been about 1.2 km diameter. We adopt this more recent value, 1.2 km, here for our calculations. Using direct comparison of kinks in the crater distribution and in the main-belt size distribution, Bottke and Chapman (2006) show that the scaling from observed crater size to probable impactor size for Mathilde is about a factor of 22.5. If this can be scaled directly to Davida, one would expect the required impactor for a 150 km crater on Davida to be about 6.4 km diameter. However, if one instead uses the same scaling as Davis (1999), given that Davida has a similar composition and is in the same collisional environment, but accounting for the gravity difference, we can extend that derivation to Davida. Scaling to the largest facet on Davida, using Eq. (4) of Davis, we find that the required impactor would be about 8.4 km in diameter. Given that it is reasonable to expect the much larger Davida (assuming similar densities, and noting that the surface gravity of Davida is approximately five times larger than Mathilde) to have more compaction, we adopt this more conservative value, 8.4 km (or about 18 times smaller than the crater), for our calculations.

Then, using the known size–frequency distribution of the main belt (Bottke et al., 2005b), we find that the number of impactors larger than 8.4 km is about 2.5% of the number larger than 1.2 km. Given that only 60% of Mathilde's surface was imaged, and that Davida has a much larger cross-section as a target, we derive that Davida should have suffered about 1.3 impacts large enough to make a crater of 150 km diameter or larger, if Davida has the same age as Mathilde. Davis indicates that Mathilde could be as young as 2 BY, based on the chances of a breakup event (requiring an impactor of size about twice that which formed the largest crater), although it is possible that it dates to the age of the Solar System (Bottke et al., 2005b). For Davida, however, the age is more straightforward. The specific energy for catastrophic disruption can be scaled from Q_D^* plots, e.g., that given by Bottke et al. (2005a). One finds that the specific energy for breakup is about 15 times larger for Davida than for Mathilde, both well into the gravity regime. The required impactor for Davida breakup, then, would be about 14 times the diameter for breakup of Mathilde, or about 35 km, scaling from the breakup size for Mathilde given by Davis. The probability of such an event over Davida's lifetime is only about 6%, and thus it is very likely that Davida dates to the age of the Solar System. Thus, it is possible that Davida may be twice as old as Mathilde (and Mathilde may have reached saturation of its large craters in half the lifetime of Davida), so we derive that Davida may have had up to about 2.5 impacts sufficient to make a 150 km or larger crater over its lifetime. The recent work of Bottke et al. (2005b) shows this (their Fig. 14) as collisional lifetimes, which is about 15 BY for Mathilde and about 32 BY for Davida. Bottke et al. (2005a) point out that it is not yet clear whether higher porosity or pre-shattered targets will affect these lifetimes either higher or lower. The chances, of course, of smaller craters, and hence smaller facets, are larger.

Therefore, the probability of getting very large craters, having diameters comparable with the body's radius, is high, and they could have accumulated without breakup of Davida. We suggest that the large facets seen on Davida are analogous to the large craters seen edge-on in the high-resolution images of Mathilde, and that such craters may be characteristic of large C-type asteroids. As pointed out by Chapman et al. (1999), the ability to retain so many large craters may reflect an inherent property of C-type asteroids in general. Such giant craters are not seen on the many S-type asteroids imaged close-up, at least not in the state of preservation of the Mathilde craters. Certainly, the densities, derived from spacecraft flyby and from observations of asteroid satellites, are systematically lower than S-types (Merline et al., 2002), and the porosities are generally

Please cite this article in press as: A.R. Conrad et al., Direct measurement of the size, shape, and pole of 511 Davida with Keck AO in a single night, Icarus (2007), doi:10.1016/j.icarus.2007.05.004

higher than for S-types (Britt et al., 2006). Our new images bolster the idea that the structure or material properties of C-type asteroids is significantly different from S-types. We hope that additional imaging, both from our ground-based program and from new spacecraft missions can continue to shed light on these differences.

7. Summary

Using adaptive optics images, obtained in a single night with the Keck II 10 m telescope, we provide improved dimensions for a triaxial ellipsoid model of main-belt C-type Asteroid 511 Davida. We find that the average diameter is about 19% smaller than had been derived from earlier techniques. Our work improves the uncertainties in the a and b dimensions by factors of about 24 and 12, respectively, relative to earlier work [e.g., Drummond and Hege (1989), who used speckle techniques].

We point out, however, that restricted viewing geometries for both our work and IRAS, make it hard to determine accurately the short dimension c. The formal quoted IRAS uncertainties of 5 km refer only to the apparent axis dimensions at the time of the observations, α and β, and do not address c. Thus caution is advised when using the IRAS diameter as an average size for Davida, since, like ours, their observations were made at rather high sub-Earth latitudes. If by average size, one means $(abc)^{1/3}$, then our 289 ± 21 km should be used. We intend to make additional observations of Davida at future critical times to determine more accurately the c dimension. With our model for shape and related phasing of the lightcurve, we can now predict good observational opportunities.

We have fortified Davida's position as a calibration standard by substantially improving its pole position, reducing uncertainties from the typical 5°–10° quoted with previous lightcurve studies, to our 2° here. The axial ratios a/b and b/c, from previous lightcurve analysis are consistent with the ratios we find here. Furthermore, we have established a latitude and longitude system on Davida, defining a prime meridian and providing a means to compute sub-Earth longitudes and latitudes at future times. We find that although Davida shows departures from a purely triaxial ellipsoid shape, it can be rather well represented by a triaxial ellipsoid, resulting in its smooth and largely featureless lightcurve.

We have identified at least three significant topographical features, two local positive relief features and one flat facet. They exhibit qualitative characteristics reminiscent of the shape of Mathilde, observed by the NEAR spacecraft in 1997 and the only C-type asteroid that has been examined in detail. Here we have taken this comparison a step further and have shown that the features seen on Davida may be analogues of the giant craters on Mathilde, and indeed may be characteristic of large C-type asteroids.

Acknowledgments

We wish to acknowledge John Cromer of the California Institute of Technology for help with early drafts of the paper, and Clark Chapman and Bill Bottke, who provided useful discussions. This work was in part supported by the NASA Planetary Astronomy grant NRA-02-OSS-01-344-32-55-05 (PI: Dumas, C). The data presented herein were obtained at the W.M. Keck Observatory, which is operated as a scientific partnership among the California Institute of Technology, the University of California and the National Aeronautics and Space Administration. The Observatory was made possible by the generous financial support of the W.M. Keck Foundation. The authors wish to recognize and acknowledge the very significant cultural role and reverence that the summit of Mauna Kea has always had within the indigenous Hawaiian community. We are most fortunate to have the opportunity to conduct observations from this mountain.

References

Asphaug, E., 2000. The large, undisturbed craters of Mathilde: Evidence for structural porosity. Lunar Planet. Sci. 31. Abstract 1864.

Bottke, W.F., Chapman, C.R., 2006. Determining the main belt size distribution using asteroid crater records and crater saturation models. Lunar Planet. Sci. 37. Abstract 1349.

Bottke, W.F., Durda, D.D., Nesvorný, D., Jedicke, R., Morbidelli, A., Vokrouhlický, D., Levison, H., 2005a. The fossilized size distribution of the main asteroid belt. Icarus 175, 111–140.

Bottke, W.F., Durda, D.D., Nesvorný, D., Jedicke, R., Morbidelli, A., Vokrouhlický, D., Levison, H.F., 2005b. Linking the collisional history of the main asteroid belt to its dynamical excitation and depletion. Icarus 179, 63–94.

Britt, D.T., Yeomans, D., Housen, K., Consolmagno, G., 2002. Asteroid density, porosity, and structure. In: Bottke, W.F., Cellino, A., Paolicchi, P., Binzel, R.P. (Eds.), Asteroids III. Univ. of Arizona Press, Tucson, pp. 485–500.

Britt, D.T., Consolmagno, G.J., Merline, W.J., 2006. Small body density and porosity: New data, new insights. Lunar Planet. Sci. 37. Abstract 2214.

Chapman, C.R., Merline, W.J., Thomas, P., 1999. Cratering on Mathilde. Icarus 140, 28–33.

Conrad, A.R., Dumas, C., Merline, W.J., Campbell, R.D., Goodrich, R.W., Le Mignant, D., Chaffee, F.H., Fusco, T., Kwok, S.A., Knight, R.I., 2006. Rotation and morphology of Asteroid 511 Davida. Lunar Planet. Sci. 37. Abstract 1955.

Davis, D.R., 1999. The collisional history of Asteroid 253 Mathilde. Icarus 140, 49–52.

Drummond, J.D., 1998. Adaptive optics Lorentzian point spread function. SPIE 3353, 1030–1037.

Drummond, J.D., 2000. Measuring asteroids with adaptive optics. In: Ageorges, N., Dainty, C. (Eds.), Laser Guide Star Adaptive Optics for Astronomy. Kluwer Academic Publishers, Dordrecht, pp. 243–262.

Drummond, J.D., 2006. Sizing up asteroids at Lick Observatory with adaptive optics. Bull. Am. Astron. Soc. 38. Abstract 59.25.

Drummond, J.D., Hege, E.K., 1989. Speckle interferometry of asteroids. In: Binzel, R.P., Gehrels, T., Matthews, M.S. (Eds.), Asteroids II. Univ. of Arizona Press, Tucson, pp. 171–191.

Drummond, J.D., Cocke, W.J., Hege, E.K., Strittmatter, P.A., Lambert, J.V., 1985. Speckle interferometry of asteroids. I. 433 Eros. Icarus 61, 132–151.

Drummond, J.D., Fugate, R.Q., Christou, J.C., Hege, E.K., 1998. Full adaptive optics images of Asteroids Ceres and Vesta; Rotational poles and triaxial ellipsoid dimensions. Icarus 132, 80–90.

Fusco, T., Mugnier, L., Conan, J.M., 2002. MISTRAL, a deconvolution algorithm for astronomical adaptive optics images. In: Combes, F., Barret, D. (Eds.), Semaine de l'Astrophysique Francaise. In: Conference Series, vol. 8. EdP-Sciences (Editions de Physique), Paris, p. 171.

Housen, K.R., Holsapple, K.A., Voss, M.E., 1999. Compaction as the origin of the unusual craters on the Asteroid Mathilde. Nature 402, 155.

Kaasalainen, M., Torppa, J., Muinonen, K., 2003. Asteroid periods, poles, and shapes from lightcurves. Icarus 164, 346–383.

Lim, L.F., McConnochie, T.H., Bell, J.F., Hayward, T.L., 2005. Thermal infrared (8–13 μm) spectra of 29 asteroids: The Cornell Mid-Infrared Asteroid Spectroscopy (MIDAS) Survey. Icarus 173, 385–408.

Magnusson, P., 1989. Pole determinations of asteroids. In: Binzel, R.P., Gehrels, T., Matthews, M.S. (Eds.), Asteroids II. Univ. of Arizona Press, Tucson, pp. 1180–1190.

Magnusson, P., Baruci, M.A., Drummond, J.D., Lumme, K., Ostro, S.J., Surdej, J., Taylor, R.C., Zappala, V., 1989. Determination of pole orientations and shapes of asteroids. In: Binzel, R.P., Gehrels, T., Matthews, M.S. (Eds.), Asteroids II. Univ. of Arizona Press, Tucson, pp. 66–97.

Merline, W.J., Howell, S.B., 1995. A realistic model for point-sources imaged on array detectors: The model and initial results. Exp. Astron. 6, 163–210.

Merline, W.J., Weidenschilling, S.J., Durda, D.D., Margot, J.L., Pravec, P., Storrs, A.D., 2002. Asteroids do have satellites. In: Bottke, W.F., Cellino, A., Paolicchi, P., Binzel, R.P. (Eds.), Asteroids III. Univ. of Arizona Press, Tucson, pp. 289–312.

Seidelmann, P.K., Archinal, B.A., A'Hearn, M.F., Cruikshank, D.P., Hilton, J.L., Keller, H.U., Oberst, J., Simon, J.L., Stooke, P.J., Tholen, D.J., Thomas, P.C., 2005. Report of the IAU/IAG Working Group on Cartographic Coordinates and Rotational Elements: 2003. Celest. Mech. 91, 203–215.

Sobel, I., 1973. On calibrating computer controlled cameras for 9 receiving 3-D scenes. In: Proc. 9th Int. Joint Conf. on Artif. Intelligence, pp. 648–657.

Veverka, J., Thomas, P., Harch, A., Clark, B., Bell, J.F., Carcich, B., Joseph, J., Murchie, S., Izenberg, N., Chapman, C., Merline, W., Malin, M., McFadden, L., Robinson, M., 1999. NEAR encounter with Asteroid 253 Mathilde: Overview. Icarus 140, 3–16.

Wizinowich, P., Acton, D.S., Shelton, C., Stomski, P., Gathright, J., Ho, K., Lupton, W., Tsubota, K., Lai, O., Max, C., Brase, J., An, J., Avicola, K., Olivier, S., Gavel, D., Macintosh, B., Ghez, A., Larkin, J., 2000. First light adaptive optics images from the Keck II telescope: A new era of high angular resolution imagery. Publ. Astron. Soc. Pacific 112, 315–319.

Please cite this article in press as: A.R. Conrad et al., Direct measurement of the size, shape, and pole of 511 Davida with Keck AO in a single night, Icarus (2007), doi:10.1016/j.icarus.2007.05.004